Confined VLS growth and structural characterization of silicon nanoribbons

Aurélie Lecestre, Emmanuel Dubois, A. Villaret, T. Skotnicki, P. Coronel, G. Patriarche, C. Maurice

Confined VLS growth and structural characterization of silicon nanoribbons

A. Lecestre [a,b,*], E. Dubois [a], A. Villaret [b], T. Skotnicki [b], P. Coronel [c], G. Patriarche [d], C. Maurice [e]

[a] IEMN – UMR CNRS 8520, Avenue Poincaré, BP 60069, 59652 Villeneuve d'Ascq, France
[b] STMicroelectronics, 850 rue Jean Monnet, 38926 Crolles Cedex, France
[c] CEA-LITEN, 17 Avenue des martyrs, 38054 Grenoble, France
[d] Laboratoire de Photonique et de Nanostructures-CNRS, route de Nozay, 91460 Marcoussis, France
[e] Ecole des Mines, Centre SMS, PECM-UMR CNRS 5146, 158 cours Fauriel, 42023 St Etienne, France

Keywords:
Vapor–liquid–solid (VLS) growth
Three-dimensional integration

A B S T R A C T

Confined VLS growth is proposed to produce single crystalline silicon (c-Si) film over an amorphous oxide layer, without crystalline seed. The guided growth of Si nanoribbons (NRs) is successfully demonstrated and characterized using several electron microscopy techniques. First, VLS growth is studied on a plane substrate covered by gold (Au) patterned parallelepipedic ingots of several dimensions. In this unconstrained growth condition, c-Si nanowires (NWs) are synthesized with controlled position but random orientation on an amorphous substrate. Subsequently, it is demonstrated that VLS growth in the spatial confinement of a cavity produces nanometer-thick c-Si blades over a micron area scale with well-controlled localization. The nature of grown silicon layers is characterized by Scanning Electron Microscopy (SEM), Electron Backscattered Diffraction (EBSD) and Scanning Transmission Electron Microscopy (STEM) to analyze its crystallinity and to check the impact of the confining cavity walls on the purity of grown silicon. This technique opens the way for the fabrication of stacked active silicon layers isolated from each other useful for 3D CMOS integration.

1. Introduction

Three-dimensional (3D) integration of semiconductor devices is presently perceived as inescapable to leverage the weight of interconnects delay latency associated to upcoming CMOS integrated circuits [1,2]. Because 3D integration requires the stacking of active layers alternated with interlayer dielectrics (ILD), the difficult challenge consists in growing crystal-quality semiconductor ribbons starting from an amorphous substrate that can obviously not initiate the necessary crystal pattern. Recently, self-assembled techniques [3–5] including the vapor–liquid–solid (VLS) [6] catalytic growth of semiconductor nanowires (NWs) has spurred a new interest on the fabrication of multi-silicon-on-insulator (multi-SOI) layers. Starting from an amorphous substrate, recent experiments show that VLS growth produces an erratic distribution of NWs size and orientation [7]. This point constitutes a major obstacle to the synthesis of position controlled crystalline wires or ribbons. As an attempt to solve this problem, the idea developed in this paper is to couple the catalytic VLS growth to a confining guide leading to the formation of nanometer-thick planar semiconductor blades over a micron area scale. Following this strategy, a confining cavity opened at one end to enable the transport of the reacting gas to a catalyst ingot positioned at the opposite closed extremity is expected to produce a crystal blade with known placement and orientation [8]. One prerequisite for implementing the proposed guided growth technique is to devise an accurate cavity fabrication technique that ensures the tight control over the size and position of the catalyst ingot and the absence of any catalyst contamination on the inner surface of its walls. Although a sacrificial Au ribbon can be used to create the empty space of the cavity by incomplete etching [8], this approach presents the risk to contaminate the grown material. To cope with this problem, the inner volume of cavities is defined by using a sacrificial germanium layer and a highly selective etching step [9]. In the rest of this paper, experimental details describing VLS growth conditions, the cavity fabrication scheme and electron microscopy characterization methods are first described. Results are subsequently presented in the following sequence: (i) A preliminary study characterizes the unconstrained growth of nanowires initiated at the surface of Au catalyst ingots in absence of a confining cavity. (ii) Results of guided growth are discussed with a particular emphasis on the impact of the cavity size on the growth mechanism. (iii) Finally, grown silicon layers are characterized by EBSD and TEM to analyze its crystalline nature [10,11] and to check the impact of the cavity walls on the material purity [12,13].

doi:10.1016/j.mee.2009.11.053

2. Experimental

VLS growth was conducted starting from Au catalytic ingots patterned on a thermally grown oxide layer of 100 nm thick over a (1 0 0)-oriented Si substrate. A 50 nm thick Au layer was deposited by e-beam evaporation without any intermediate adhesion layer and was structured into ingots by lift-off after e-beam lithography over a positive-tone resist. The VLS process was performed in a LPCVD reactor at 500 °C, using 5% silane (SiH_4) diluted in H_2/Ar as silicon precursor at flow rate of 100 sccm, under a total pressure 0.5 mbar. Two growth configurations were subsequently considered and were associated to the unconstrained growth (Fig. 1) and to the guided growth in a cavity (Fig. 2), respectively. To control the position and dimensions of cavities and of catalyst ingots independently from one another, the cavity fabrication is based on the etching of a patterned sacrificial Ge layer. The detailed fabrication process is described in Fig. 2a. In order to properly observe NRs after confined growth, a de-processing step is necessary to selectively remove the top and lateral cavity walls without damaging the underlying materials. In this context, the role of the Si_xO_y liner is to provide selectivity for the necessary etching steps. The nitride capping composing the cavity walls is etched by reactive ion etching and the oxide liner is finally eliminated by wet etching in hydrofluoridric acid. Structural properties of Si NRs are studied by EBSD and TEM. For top view TEM observations, samples have been prepared after the etching of the cavity sidewalls, of the Au residues and of the SiO_2 thermal layer between the Si and substrate. Si NRs have been peeled off with a micropipette and deposited on a TEM grid to enable STEM observations under bright field (BF) and high angle annular dark field (HAADF) conditions.

3. Results

3.1. Localized Si NWs growth on amorphous substrate

The use of an amorphous substrate, the volume of the catalyst ingot, the dimensions of the cavities as well as the growth temperature and related gas flow and pressure (less than 600 °C when 3D MOS integration is considered) constitutes operational coupled constraints that can severely impact the final result. In order to check that these parameters are compatible with VLS in free condition, a preliminary study has been performed to characterize the unconstrained growth. A plane amorphous substrate with Au catalyst ingots of identical dimensions than those used for guided growth (50 nm thick and from 50 nm to 2 μm wide) were considered for that sake (Fig. 1). Using the aforementioned growth conditions, Si NWs were obtained only for the smallest Au ingots (50×50, 100×100 and 200×200 nm^2). For larger dimensions (0.5×0.5, 1×1 and 2×2 μm^2), a mixture of Au and Si was observed without NWs growth. Fig. 1 reveals that the diameter and the position of Si NWs can be controlled by the initial position of the catalyst. However, NWs present a random orientation and Au diffusion on Si NWs sidewalls is clearly observed [12,13]. One important outcome of this preliminary study is the observation of crystalline NWs growth providing that the initial 50 nm thick Au ingots have lateral dimensions smaller than 200 nm, for the specified growth conditions (500 °C, 5% SiH_4 in H_2/Ar, 0.5 mbar).

3.2. Si NRs growth inside cavities

A schematic description of the confining cavities is given in Fig. 2a. During growth, silane penetrates into the cavity, reacts with the Au forming a liquid Au_xSi_y alloy at the back of this cavity. Following the VLS mechanism, crystalline Si precipitates at the interface between the alloy and the cavity sidewall. Overall, the catalytic growth was successful for cavities featuring large dimensions: 50 nm thick, 10, 5 and 2 μm long, and for widths in the 200 nm to 2 μm range. Fig. 2b and c shows one typical example of cavities (10 μm long and 1 μm wide) before and after the VLS growth. Both long (2 μm) and short (50 nm) Au ingots successfully catalyzed Si growth. Moreover, the presence of an Au drop at the tip of every NRs tends to confirm VLS growth took place. In order to control the dimensions and orientation of Si NRs with precision,

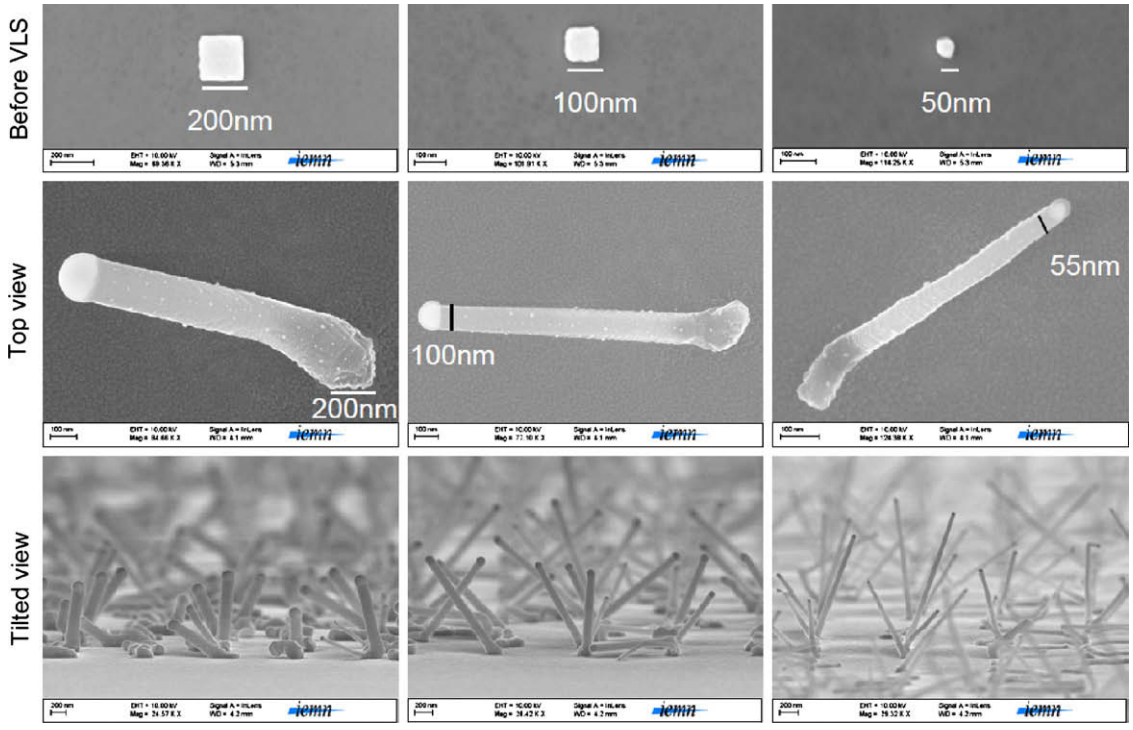

Fig. 1. Unconstrained localized growth and influence of the catalyst ingots dimensions on the VLS growth: SEM images (top and tilted view) of Au slugs (50×50, 100×100 and 200×200 nm^2) on a plane amorphous substrate, before and after growth.

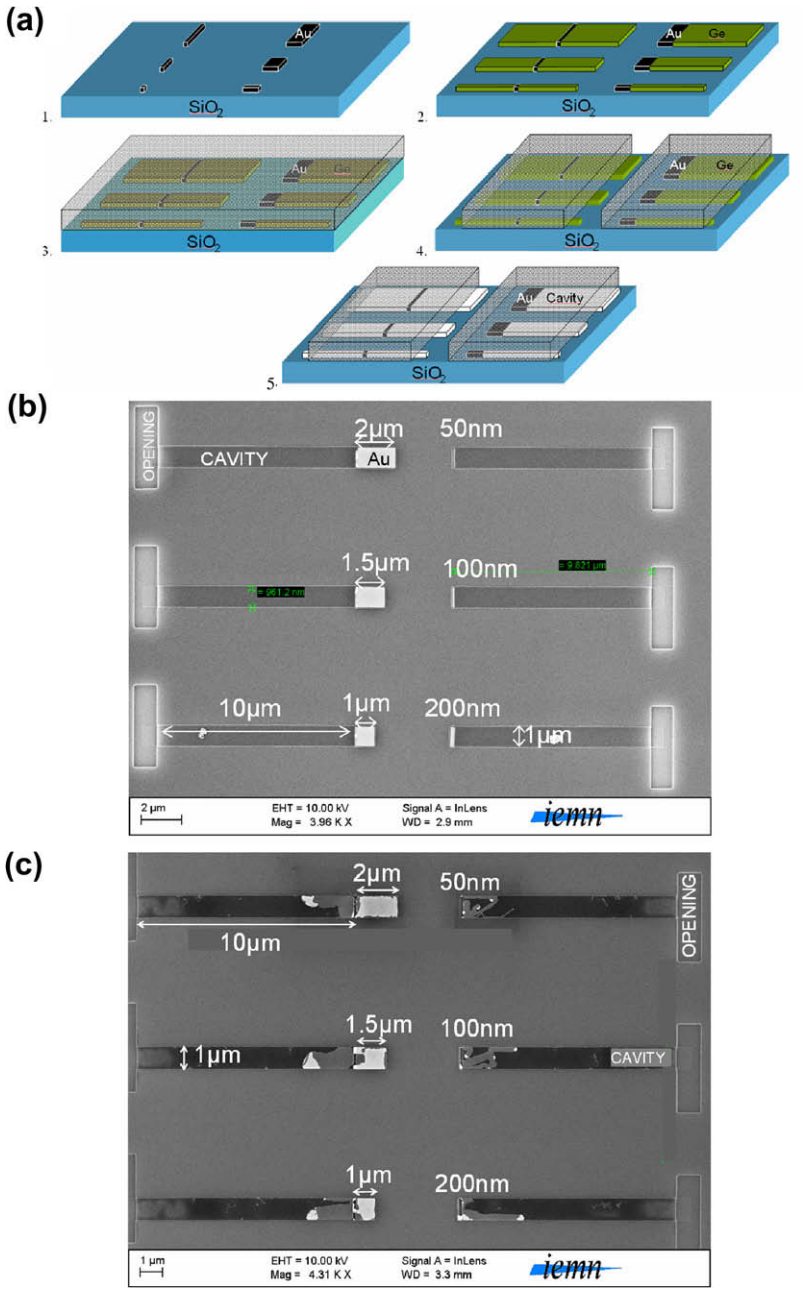

Fig. 2. (a) Schematic representation of confining cavities using for guided VLS growth. (1) Patterning of catalyst Au ingots by e-beam lithography and lift-off. (2) Formation of sacrificial Ge strips aligned to catalytic ingots by e-beam lithography and a second lift-off step. These strips define the cavity dimensions. (3) SiO_x liner deposition and formation of a SiN conformal capping by PECVD. (4) Opening of the cavity extremity by lithography and RIE. (5) Selective wet etching of the sacrificial Ge lines. (b) Cavities before VLS growth: SEM image (top view) of several cavities (50 nm thick, 10 µm long and 1 µm wide), containing Au catalyst ingots of different lengths at their closed extremity (from 50 nm to 2 µm). (c) SEM image (top view) of the same cavities after VLS growth (500 °C, 5% SiH_4, 100 sccm, 30 min). The SiN cavities walls (cap layer) were selectively etched to free the Si nanoblades. As in the case of nanowires growth, the catalyst is pushed by the front of crystal growth. For long catalyst slugs, part of it remains at the initial position in the back of the cavity.

it is worth noting that cavities with a width of 200 nm or less are the most suitable. For wider cavities, growth takes place under the form of several NWs in parallel without being guided by the sidewalls (Fig. 2c). This observation is in agreement with the growth of Si NWs on a plane substrate. Beyond the catalytic dissociation of silane in the cavity, its thermally induced decomposition also produces the formation of an amorphous silicon layer that deposits over the entire surface of the sample. One consequence is the reduction of the gas flow at the cavity entrance. Another drawback is the concentration reduction of reactive gas because its decomposition generates a by-product (H_2) that must be evacuated through the cavity entrance which also feeds the reaction with silane. This point is consolidated by Fig. 3a which clearly outlines growth rate reduction with time. AFM views in Fig. 3c confirm that amorphous Si is deposited inside the cavity with an average thickness of 40 nm and RMS roughness of 8 nm.

3.3. Structural analysis of Si NRs

Fig. 4 shows a typical EBSD analysis performed on a 200 nm wide Si NR obtained by confined VLS growth in a cavity. This analysis confirms the formation of a single crystal, and in this particular case, the

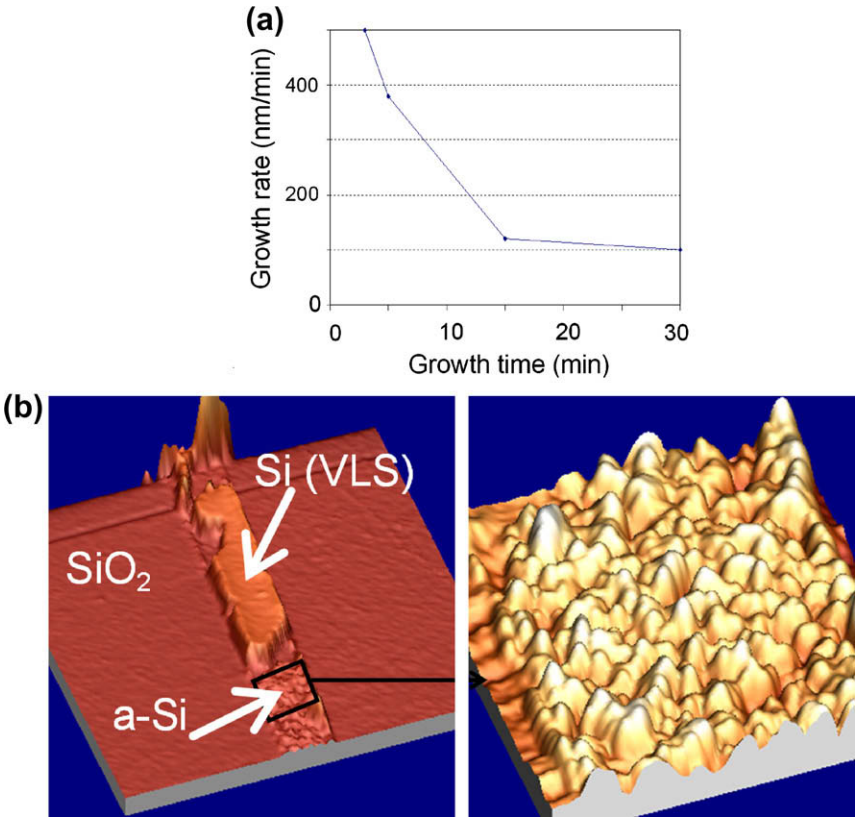

Fig. 3. (a) Graph showing the evolution of the crystalline Si NR growth rate as a function of the growth time. Growth conditions: 500 °C, 0.5 mbar, 5% SiH_4 in H_2/Ar, 100sccm. (b) AFM image of the Si NR topography, with a zoom on amorphous Si deposited inside the cavity during VLS growth.

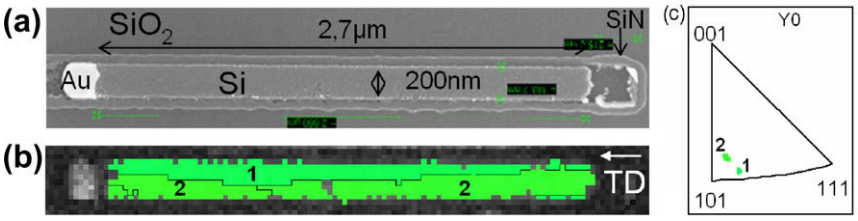

Fig. 4. EBSD analysis showing the crystallinity of the whole Si NR grown inside a cavity (50 nm thick, 200 nm wide). (a) SEM image of a Si NR grown by VLS inside a cavity, after the etching of the cavity walls (cap layer). (b) Crystal orientation map provided by EBSD analysis, revealing two main orientations indexed 1 and 2. (c) Inverse pole figure corresponding to view (b) in the transverse direction (TD) of the blade that reveals a dominant direction of growth close to [1 0 1].

presence of twinned domains. The mapping of crystal orientation associated to the inverse pole figure in the transverse direction (TD) parallel to the NRs length reveals a dominant growth direction close to [1 0 1]. However, it remains difficult to quantitatively ascertain this information because the epitaxial growth does not necessarily follows the alignment of the cavity. Complementary to EBSD analysis, top view TEM characterizations have been performed in order to investigate the occurrence of crystalline defects, to determine the growth direction and to detect gold contamination. Fig. 5a shows one example of Si NR characterized by STEM under the ⟨1 1 0⟩ zone axis. The multi-twinned structure of the Si blade is clearly evidenced. The second image (Fig. 5b) in BF STEM reveals three twinned domains with their respective {1 1 1}-oriented boundary planes. Dumbbells with Si–Si atoms aligned along the ⟨0 0 4⟩ direction and separated by 0.136 nm can be clearly identified while the 180° rotation between two twinned planes is easy to distinguish. Finally, the result of HAADF characterization shown in Fig. 5c reveals the presence of Au contamination that takes the form of clusters located at the surface of NRs.

4. Conclusion

The work presented in this paper shows that the VLS growth technique can be used to produce crystalline thin silicon films on an amorphous substrate at a temperature as low as 500 °C. A preliminary study has been performed on the localized VLS growth of Si NWs on amorphous substrate. These experiments showed that Au catalytic ingots generate crystalline silicon. However, their lateral dimensions have to be less or equal to 200 nm to control the NW diameter. Similar observations have been done for the guided VLS growth. Moreover, the crystalline nature of the grown Si NR has been evidenced by STEM and EBSD analyses for the first time. Localized and oriented growth of semiconductor crystal on an amorphous substrate opens new perspective for stacking independent and isolated Si crystal-quality layers for 3D CMOS integration. Nevertheless, guided VLS growth still requires further optimization to prevent uncontrolled gold diffusion in the cavity so that defect-free crystalline Si ribbons can be properly grown.

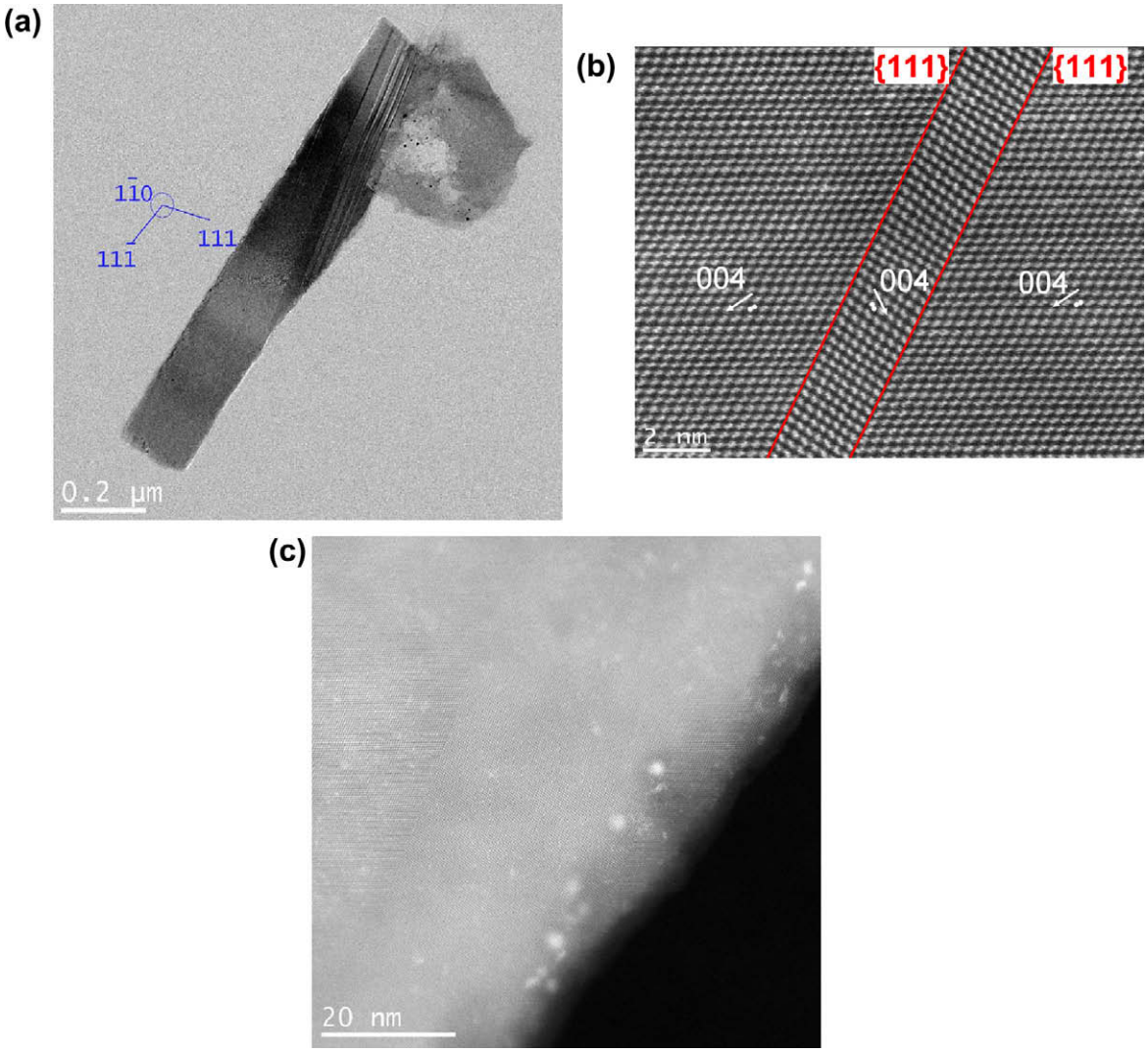

Fig. 5. STEM analysis showing the crystalline nature of silicon grown by VLS. (a) Bright field-STEM (top view) of the whole Si nanoribbon under the ⟨1 1 0⟩ zone-axis diffraction condition that reveals the multi-twinned structure of the Si blade. (b) High-resolution BF image showing details of a twin boundaries taking place at {1 1 1} planes. Si–Si dumbbells are materialized by yellow dots. (c) HAADF–STEM image revealing Au clusters on the NR sidewalls.

References

[1] K. Sakuma, P.S. Andry, C.K. Tsang, S.L. Wright, B. Dang, C.S. Patel, B.C. Webb, J. Maria, E.J. Sprogis, S.K. Kang, R.J. Polastre, R.R. Horton, J.U. Knickerbocker, IBM J. Res. Dev. 52 (2008) 611–622.

[2] H. Lim, S.M. Jung, Y. Rah, T. Ha, H. Park, C. Chang, W. Cho, J. Park, B. Son, J. Jeong, H. Cho, B. Choi, K. Kim, Proc. IEEE (2005) 549–552.

[3] T. Shimizu, Z. Zhang, S. Shingubara, S. Senz, U. Gösele, Nano Lett. 9 (2009) 1523–1526.

[4] T. David, D. Buttard, M. Den Hertog, P. Gentile, T. Baron, P. Ferret, J.L. Rouvière, Superlattices Microstruct. (2007).

[5] M. Gowtham, L. Eude, B. Marquardt, A.Q.L. Quang, C.S. Cojocaru, P. Legagneux, D. Pribat in: Proceeding Synthesis and Integration of New Materials (Th-M3). JNTE, Toulouse, 2008.

[6] R.S. Wagner, W.C. Ellis, Appl. Phys. Lett. 4 (1964) 89–90.

[7] S. Akhtar, A. Tanka, K. Usami, Y. Tsuchiya, S. Oda, Thin Solid Films 517 (2008) 317–319.

[8] Y. Shan, A.K. Kalkan, C.Y. Peng, S.J. Fonash, Nano Lett. 4 (2004) 2085–2089.

[9] A. Lecestre, E. Dubois, A. Villaret, P. Coronel, T. Skotnicki, D. Delille, C. Maurice, D. Troadec, IOP Conf. Series: Mater. Sci. Eng. 6 (2009) 012022.

[10] B. Chen, J. Chen, T. Sekiguchi, M. Saito, K. Kimoto, J. Appl. Lett. 105 (2009) 113502.

[11] C. Cayron, M. Den-Hertog, L. Latu-Romain, C. Mouchet, C. Secouard, J.L. Rouviere, E. Rouviere, J.L. Simonato, Appl. Crystallogr. 42 (2009) 242.

[12] J.B. Hannon, S. Kodambaka, F.M. Ross, R.M. Tromp, Nature 440 (2006) 69–71.

[13] J.E. Allen, E.R. Hemesath, D.E. Perea, J.L. Lensch-Falk, Z.Y. Li, F. Yin, M.H. Gass, P. Wang, A.L. Bleloch, R.E. Palmer, L.J. Lauhon, Nat. Nanotechnol. 3 (2008) 168–172.